

Coverage dependent desorption kinetics of CO from Rh(111): a theoretical analysis

S.H. Payne, H.J. Kreuzer

Department of Physics, Dalhousie University, Halifax, Nova Scotia, Canada B3H 3J5

K.A. Peterlinz, T.J. Curtiss, C. Uebing¹ and S.J. Sibener

The James Franck Institute and The Department of Chemistry, The University of Chicago, Chicago, IL 60637, USA

Received 14 October 1991; accepted for publication 17 January 1992

For a triangular lattice gas with up to third-nearest neighbor interactions between CO molecules adsorbed on Rh(111), we calculate the desorption kinetics assuming quasi-equilibrium throughout the desorption process. These calculations are compared with linearized and essentially isosteric kinetic data that were obtained using a three molecular beam scattering arrangement. The experimental desorption rates and ordered adsorbate structure data, including phase transition temperatures, are accurately reproduced using transfer matrix calculations. From these calculations we obtain quantitative values for inter-adsorbate interactions extending out to third-nearest neighbor distances. Standard Monte Carlo simulations qualitatively show the correct trends in the coverage dependent rate data, but are quantitatively inadequate for this system since the wrong coverage dependence of the sticking coefficient is implicitly assumed.

1. Introduction

Measurement and modelling of the coverage dependence of equilibrium and non-equilibrium data for adsorbates have become essential for understanding surface processes. Practical applications, such as catalysis or thin film growth, occur over a wide range of coverages, and the underlying processes such as diffusion, adsorption, desorption, or adsorbate reconstruction are increasingly affected by lateral interactions as the coverage increases. Such effects are already observed in single adsorbate systems [1–7].

For systems in which surface diffusion is so fast that the adsorbate remains in quasi-equilibrium throughout desorption, the desorption rate is given in terms of the coverage dependent

sticking coefficient and the chemical potential. Thus one model for the lateral interactions in the adsorbate should suffice to reproduce experimental data on both equilibrium and kinetic properties. This approach differs significantly from previous model calculations that typically were concerned with one observable property only, i.e., phase diagrams or kinetics. To calculate the chemical potential, the lattice gas model has been used extensively. Whereas early calculations were based on cluster variation schemes [8,9], there are now essentially exact methods available based on either Monte Carlo simulations [10] or transfer matrix techniques [11–13]. The latter has recently been demonstrated as a fast and efficient method for calculating phase diagrams and equilibrium properties for systems with both pairwise and multi-particle interactions.

In a recent paper [14] coverage dependent desorption measurements of CO from Rh(111) were presented. In addition to the reported de-

¹ Present address: Institut für Festkörperforschung, Forschungszentrum Jülich, Germany.

sorption rates, the measured He diffraction data, the specular helium scattering versus CO coverage, and the coverage dependent sticking coefficient all indicated nearest neighbor repulsive interactions between co-adsorbed CO molecules. From the kinetic data and the sticking coefficient, an expression for the chemical potential was determined. The variation of the chemical potential with coverage suggested that additional, even longer range adsorbate interactions significantly affect the desorption kinetics. With the coverage dependent desorption data, the many studies of ordered adsorbate structures, including temperature dependent $1/3$ ML diffraction data, the coverage dependent sticking coefficient, and data for the coverage dependence of adsorption sites, this system is well characterized and a good candidate for model calculations.

In the next section we summarize experimental results on the desorption kinetics and the structural data for CO on Rh(111). In section 3 we present the results of the transfer matrix calculation of the desorption rates, determining the set of lateral interaction parameters that give an excellent overall fit to structural and kinetic data with a 3.38 kcal/mol nearest neighbor repulsion, a 0.338 kcal/mol next-nearest neighbor repulsion, and a 0.169 kcal/mol third-nearest neighbor attraction. In section 4 we discuss results from Monte Carlo simulations of structural features which qualitatively show that nearest neighbor and next-nearest neighbor interactions must both be repulsive. However, simulations of desorption kinetics are limited in that the standard assumption for the sticking coefficient, namely $S(\theta) = S_0(1 - \theta)$, is not valid for this system.

2. Experimental results

We present here a summary of relevant experimental results from ref. [14]. He diffraction scans from the $1/3$ monolayer overlayer of CO on Rh(111) were consistent with a $(\sqrt{3} \times \sqrt{3})R30^\circ$ overlayer at surface temperatures below 325 K, and diffraction peaks disappeared with no loss of CO coverage for $325 < T_s < 380$ K (see fig. 1). We note that these diffraction measurements

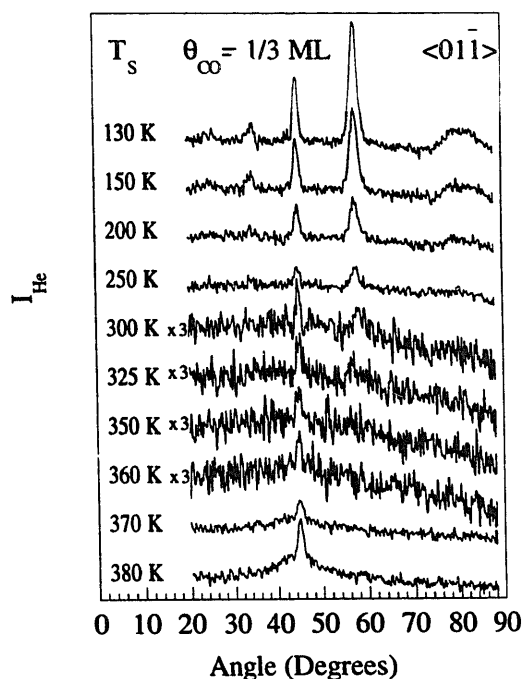


Fig. 1. Shown are He diffraction curves for a $\theta_i = 45^\circ$, $E_i = 63$ meV He beam along the $\langle 01\bar{1} \rangle$ azimuth. At $T_s = 130$ K, peak positions agree well with those expected from the established $(\sqrt{3} \times \sqrt{3})R30^\circ$ CO/Rh(111) $1/3$ ML ordered overlayer, with the (0,0) peak at 45° and the larger $(1/3, 2/3)$ peak at 59° . As the surface temperature is increased, the diffraction pattern disappears until at 325 K no diffraction is visible. If the overlayer is heated quickly (in approximately 1 min) to 380 K and immediately cooled back to 130 K, the diffraction pattern is reproduced, demonstrating that a disordered $1/3$ ML phase exists between 325 and 380 K. (Reproduced with permission from ref. [14].)

confirmed the nearest top site neighbor lattice spacing of 2.69 Å, the next-nearest top site neighbor spacing of 4.65 Å, and the third nearest top site neighbor spacing of 5.37 Å between top sites on Rh(111). No diffraction peaks were observed with lower coverages of CO and temperatures down to 130 K. Combined with information from an EELS study by Dubois and Somorjai [15], these results indicate that CO existed in a disordered phase, primarily adsorbed on top sites, for coverages below $1/3$ and temperatures above 325 K.

CO desorption kinetics were measured with a three molecular beam apparatus [14,16–18] which incorporated specular He scattering with two CO

beams, one modulated and weak, the other continuous and intense, in order to linearize the kinetics. While the intense beam set a steady state coverage, the weak beam perturbed that coverage. CO coverages were calibrated as a function of specular He scattering intensity at several temperatures in the range $325 < T_s < 380$ K. The resulting calibration function was well characterized by a temperature independent model that assumes CO is randomly distributed and has a 148 \AA^2 He scattering cross section [14]. CO coverages and induced coverage modulations were determined from the changes in He scattering intensity or reflectivity. Since the measured first order relaxation rates were different from the actual desorption rates, corrections were applied to the measured rates to account for contributions from the first derivative of the observed sticking coefficient, $S_0(1 - 3\theta)$, and the first derivative of the rate constant, with respect to coverage [14]. We note that this three molecular beam arrangement provides a generalized approach for measuring coverage dependent surface kinetics under linearized and essentially isosteric conditions (see ref. [14] for details).

3. Desorption rate analysis

For systems in which surface diffusion is sufficiently rapid that the adsorbate remains in quasi-equilibrium during desorption, the desorption rate is given by

$$\left. \frac{d\theta}{dt} \right|_{\text{des}} = -S(\theta, T) a_s \frac{k_B T}{h \lambda_{\text{th}}^2} \exp(\mu_a / k_B T), \quad (1)$$

$S(\theta, T)$ is the sticking coefficient, a_s is the area of one adsorption site, and $\lambda_{\text{th}} = h / (2\pi m k_B T)^{1/2}$. The chemical potential, $\mu_a(\theta, T)$, of the adsorbate depends implicitly on the interactions between the adsorbed particles, as well as their bonding to the substrate. If μ_a is calculated for a given set of parameters, eq. (1) can be employed to calculate the desorption kinetics, e.g. in the form of desorption isosteres which can then be compared

directly to the experimental plots of rate constant versus $1/T$. Such isosteres are then conveniently parameterized according to Frenkel–Arrhenius as

$$\left. \frac{1}{\theta} \frac{d\theta}{dt} \right|_{\text{des}} = -\nu_{\text{eff}}(\theta, T) \exp(-E_d(\theta, T) / k_B T) \quad (2)$$

defining the desorption energy, $E_d(\theta, T)$ and the effective prefactor $\nu_{\text{eff}}(\theta, T)$. We note that under quasi-equilibrium conditions the desorption energy is related to the isosteric heat of adsorption by

$$E_d(\theta, T) = Q_{\text{iso}}(\theta, T) - k_B T / 2 + k_B T^2 \frac{\partial \ln(S(\theta, T))}{\partial T}, \quad (3)$$

where the latter can be determined independently from adsorption isotherms as

$$Q_{\text{iso}}(\theta, T) = k_B T^2 \left. \frac{\partial \ln P}{\partial T} \right|_{\theta}, \quad (4)$$

where P is the gas pressure above the surface. Note that ν_{eff} includes the sticking coefficient, $S(\theta, T)$. We reiterate that for CO/Rh(111), the coverage dependence has been measured to be $S(\theta) = 1 - 3\theta$ for $0 < \theta < 0.22$ [14]. Details of the theory underlying thermal desorption can be found in ref. [19].

To calculate $\mu_a(\theta, T)$ we use a lattice gas model which assumes on-top site adsorption on a triangular lattice. The Hamiltonian is

$$H = E_s \sum_{i=1}^N n_i + V_2 \sum_{ij} n_i n_j + V_2' \sum_{(ij)'} n_i n_j + V_2'' \sum_{(ij)''} n_i n_j. \quad (5)$$

Here $n_i = 0$ or 1 , E_s is the single adparticle (site) energy, and V_2 , V_2' , and V_2'' are the two-particle interaction strengths between nearest (ij) , next-nearest $(ij)'$, and third-nearest $(ij)''$ neighbors. We specify

$$E_s = -V_0 - k_B T \ln(q_3 q_{\text{int}}), \quad (6)$$

where V_0 is the (positive) binding energy of the isolated particle on the surface; $q_3 = q_z q_{xy}$ is its site vibrational partition function with

$$q_z = \exp(hv_z/2k_B T) / [\exp(hv_z/2k_B T) - 1], \quad (7)$$

its component for motion perpendicular to the surface. A similar expression applies for the in-plane component, q_{xy} , in the case of a localized adsorbate. q_{int} takes account of any internal degrees of freedom of the adsorbed particles, e.g. frustrated rotations in the case of CO molecules. The coverage, θ , of the system follows from the grand canonical partition function $\Xi(T, N_s, \mu_a)$ for N_s sites

$$\theta = \frac{1}{N_s} \sum n_i = \frac{k_B T}{N_s} \left. \frac{\partial \ln \Xi}{\partial \mu_a} \right|_T. \quad (8)$$

To calculate Ξ we apply the finite-size transfer matrix method to a $(M \times \infty)$ lattice [13,20,21] in which one correctly counts the bonds between two adjacent columns of M sites each. For sufficiently large M , the method gives essentially exact results. For the triangular lattice corresponding to on-top adsorption sites on Rh(111) we have constructed the transfer matrix containing the interaction of four neighboring columns of M sites to properly include the bonds represented in (5) and have chosen $M = 6$ for manageable computations.

We now present results for isosteric plots of the desorption rate, and E_d and v_{eff} , for various sets of parameters. The site energy parameters, V_0 and $v_{i=z,xy}$, of (6) can be found from the experimental desorption isosteres as follows: the slope and intercept of the lowest coverage isostere ($\theta < 0.003$) at the highest temperature recorded ($T_1 \approx 560$ K), where CO interactions are insignificant, fixes $E_d(\theta = 0, T_1)$ and $v_{\text{eff}}(\theta = 0, T_1)$, respectively, via eq. (2). However, eq. (1) with μ_a determined by E_s in eqn. (5) alone, for $\theta = 0$, is the proper description of this isostere at temperature T_1 . With the assumption that $v_z = v_{xy}$, the quantities V_0 and v_i are uniquely determined. We find $E_d(\theta = 0, T = 560 \text{ K}) = 33.6 \text{ kcal/mol}$ and $v_{\text{eff}}(\theta = 0, T = 560 \text{ K}) = 4.28 \times 10^{14} \text{ s}^{-1}$, giving $V_0 = 34.2 \text{ kcal/mol}$ and $v_i = 6.13 \times 10^{12} \text{ s}^{-1}$, $i = z,$

xy . (We neglect the contribution of frustrated rotations for simplicity – their inclusion will lower v_i above.) We note here that the above values for $E_d(\theta = 0)$ and $v_{\text{eff}}(\theta = 0)$ are different from those quoted in ref. [14] due to the exclusion of a single datum at $1000/T = 1.78 \text{ K}^{-1}$. The overall rates are essentially the same.

We start with a model with nearest-neighbor repulsion only (i.e., $V_2' = V_2'' = 0$). Although such repulsion for CO adsorbed on fcc faces of transition metals is well known, magnitudes from ab initio calculations are not particularly reliable. We arrive at an estimate by associating the disappearance of the $(\sqrt{3} \times \sqrt{3})R30^\circ$ structure observed in He beam diffraction at $T = 325$ K and $\theta = 1/3$ with the disordering temperature for this structure, which occurs at $k_B T_c \approx 0.34 V_2$ [22]. This gives $V_2 \approx 960$ K. In fig. 2a we plot the resulting first-order desorption rate constants with the experimentally determined rate constants for comparison. From fig. 2a, we see that this interaction alone gives a poor fit to the experimental rate isosteres.

Because the model isosteres are insufficiently spread in $1/T$, as compared to experiment, we are lead to try a much larger repulsion. In fig. 2b we have increased the repulsion to $V_2 = 5400$ K, which is essentially infinite compared to the temperatures of interest (the hard hexagon model [22]). Now the desorption energy remains constant up to saturation at $\theta = 1/3$. Again, however, the spread of isosteres is less than that of the experiment. We emphasize that the decrease of the sticking coefficient also controls the spread of isosteres in the Arrhenius plot. One could achieve a fit to the isosteres by choosing the sticking coefficient $S(\theta) = 1 - \rho\theta$, $1 < \rho < 2$, but this is of course unphysical since the sticking coefficient has been independently determined in another experiment [14]. Thus we conclude that nearest neighbor repulsion, however strong, is not sufficient to fit the desorption rate.

To increase the repulsion between the CO molecules we must include, at a minimum, the next-nearest neighbor term in the Hamiltonian, $V_2' > 0$. In fig. 3 we display good fits to the isosteric data obtained for two choices, expressed in terms of the ratio $R = V_2'/V_2$, namely $V_2 =$

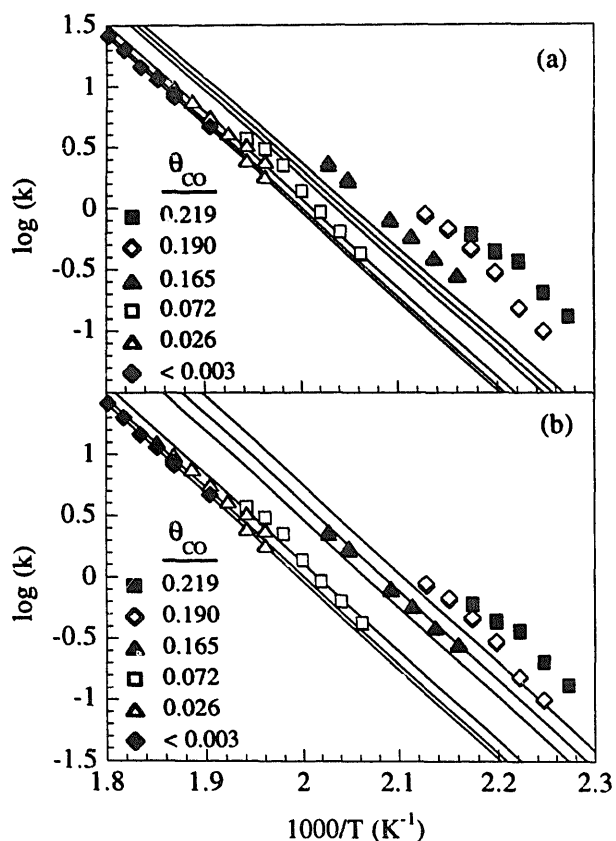


Fig. 2. Shown in each panel as symbols are experimentally determined desorption rate constants for each indicated coverage following the procedure of ref. [14]. The lines in the two panels are isotherms corresponding to the indicated coverages and calculated according to eq. (1). In panel (a), (nearest neighbor repulsion) $V_2 = 960$ K (1.9 kcal/mol), and in panel (b), $V_2 = 5400$ K (essentially a hard core repulsion).

1400 K, $R = 0.1$ and $V_2 = 1200$ K, $R = 0.2$. We will show that structural information at low temperatures is sufficient to exclude parameter sets with $R = 0.2$ from further consideration. We have also performed calculations with the addition of a third-nearest neighbor attraction. For the values $V_2 = 1700$ K, $R = 0.1$, and $R' = V_2''/V_2 = -0.05$, we see in fig. 4 an improved fit to the highest coverage data and an equally good fit to the rest of the data when compared to fig. 3. The uncertainty in the values of V_2 in these fits is no more than 10%, reflecting the extent of the experimental uncertainty in the high coverage isotherms. In fig. 5 we display the coverage- and temperature-dependent desorption energy and prefactor for the parameters of fig. 4. The origin of the cover-

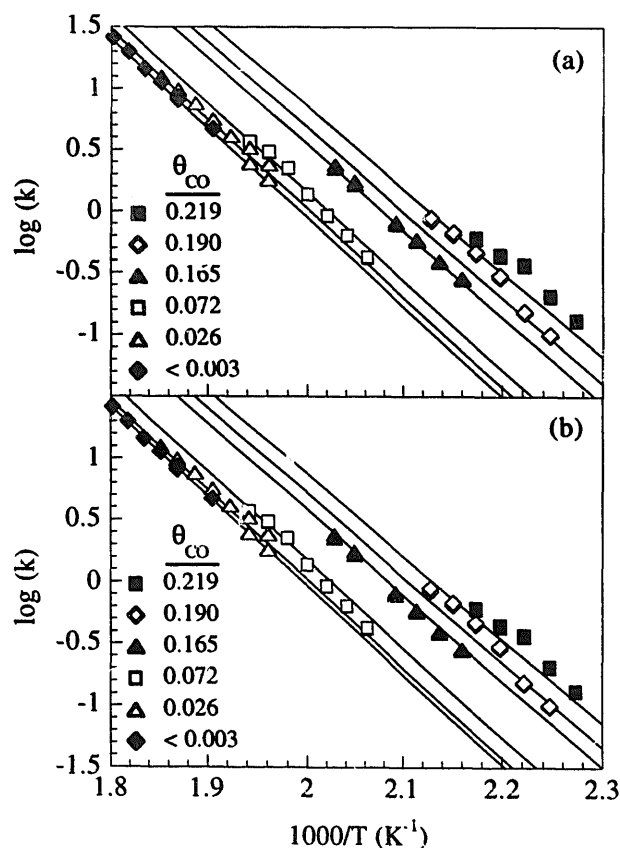


Fig. 3. The symbols and lines have the same meaning as in fig. 2. In panel (a), $V_2 = 1400$ K (2.78 kcal/mol) and (next-nearest neighbor repulsion) $V_2' = 0.1V_2$ (0.28 kcal/mol), and in panel (b), $V_2 = 1200$ K (2.38 kcal/mol) and $V_2' = 0.2V_2$ (0.476 kcal/mol).

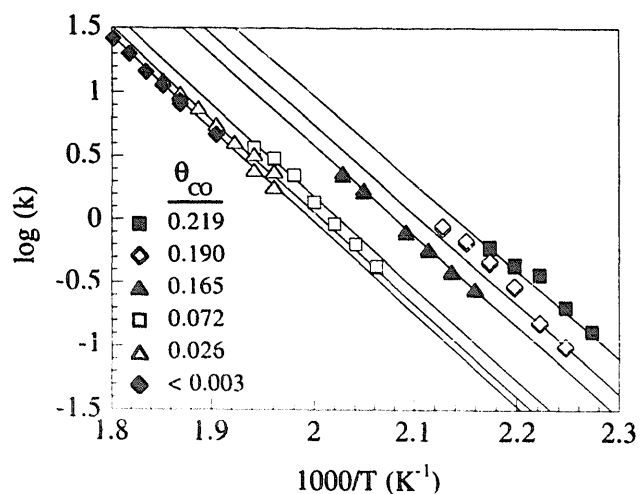


Fig. 4. The symbols and lines have the same meaning as in fig. 2. The CO interactions are $V_2 = 1700$ K (3.38 kcal/mol), $V_2' = 0.1V_2$ (0.34 kcal/mol), and (third-nearest neighbor) $V_2'' = -0.05V_2$ (-0.17 kcal/mol).

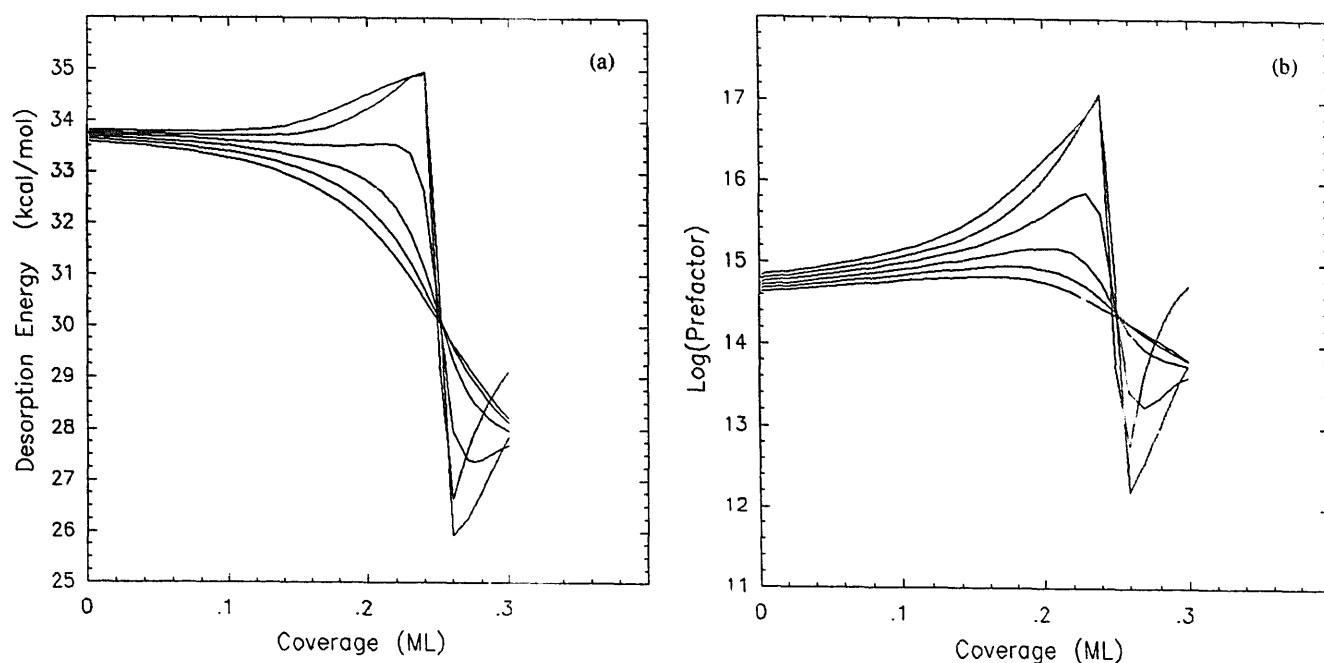


Fig. 5. Here (a) desorption energy (kcal/mol) and (b) logarithm of corresponding prefactor (as defined by eq. (2)) are plotted as functions of coverage and temperature for the interaction parameters of fig. 4. Curves correspond to the temperatures (top to bottom at $\theta = 0.2$) $T = 260, 320, 380, 440, 500,$ and 560 K. The sticking coefficient $S(\theta) = 1 - 3\theta$ is included in the calculation of the prefactor.

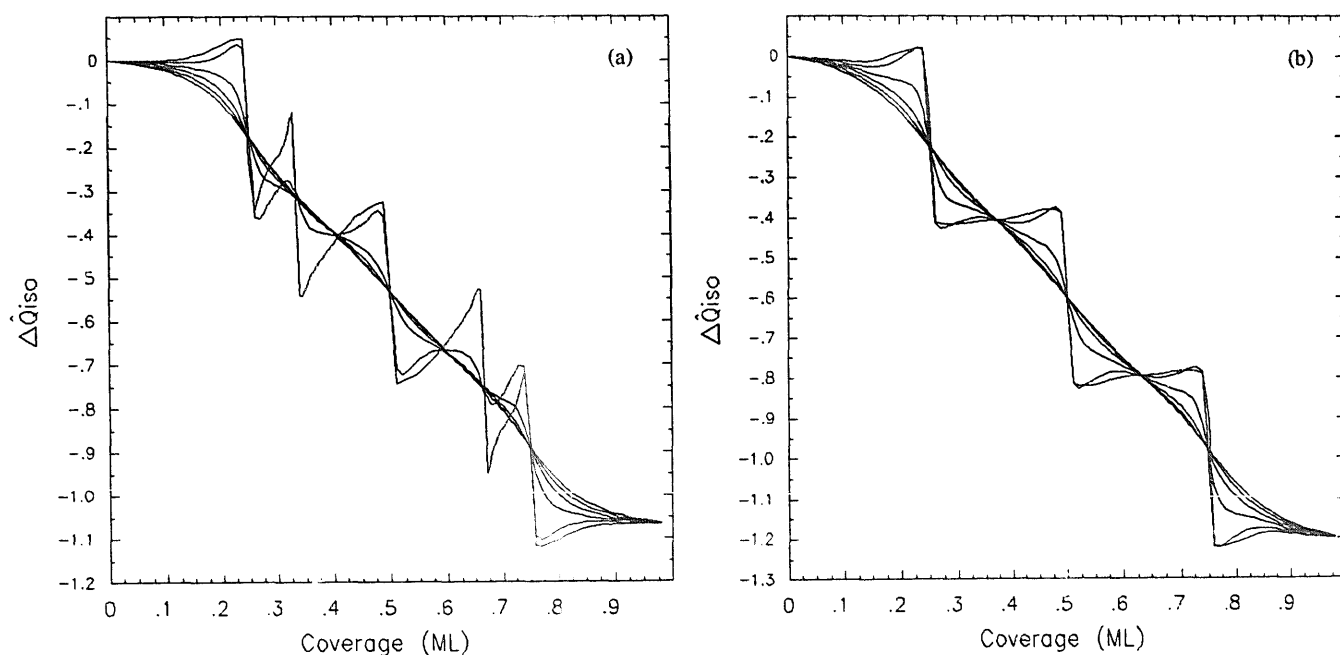


Fig. 6. Normalized isosteric heats of adsorption are plotted here as a function of coverage and reduced temperature, T/V_2 . Temperature values are (top to bottom at $\theta = 0.2$) $T/V_2 = 0.15, 0.20, 0.25, 0.30, 0.35,$ and 0.40 . In (a), $V_2' = 0.1V_2$ and $V_2'' = -0.05V_2$ were used to calculate $\Delta\hat{Q}_{iso}$, and in (b), $V_2' = 0.2V_2$ was used.

age dependence of $E_d(\theta, T)$ is discussed below with reference to fig. 6. However, the partial compensation of $E_d(\theta, T)$ and $v_{\text{eff}}(\theta, T)$ is noteworthy. The variation of these quantities with temperature at zero coverage arises from that of eq. (6). We note that trio interactions, including nearest-neighbor and next-nearest neighbor sites, could also be included in a more general Hamiltonian, but they should have negligible effect below coverages $\theta < 1/3$.

Our conclusions concerning the sign of V'_2 and its probable magnitude disagree with those of Kjoll et al. [23] for this system. They modeled the ordered structures at low coverage ($\theta < 1/3$) and low temperature ($T < 125$ K) observed by Thiel et al. [24] in a LEED study, namely a $(\sqrt{3} \times \sqrt{3})R30^\circ$ pattern, with maximum intensity at $\theta = 1/3$, and a weak (2×2) pattern at coverage $1/4$. (Because of their experimental arrangement, Thiel et al. could not definitely conclude that this was a true (2×2) pattern.) Kjoll et al. [23] calculated phase diagrams assuming infinite nearest neighbor repulsion ($V_2 = \infty$), and second and third nearest neighbor attraction ($V'_2, V''_2 < 0$). In particular, they were able to produce a disordered phase, ordered $p(2 \times 2)$ and $(\sqrt{3} \times \sqrt{3})R30^\circ$ phases, and/or coexistence of these for $T/V'_2 > 4$, and for two ratios $R'/R = 3$ and 7.4 . We have checked Kjoll's model parameters by adding these attractive interactions to the hard hexagon model and found that the desorption isosteres *cannot* be fit satisfactorily. However, we have strong evidence that the phases observed by Thiel et al. [24] can be obtained for finite V_2 and repulsive V'_2 values *similar* to those which produced figs. 3 and 4.

In fig. 6 we graph a normalized isosteric heat of adsorption

$$\Delta \hat{Q}_{\text{iso}} = \frac{1}{6V_2} [Q_{\text{iso}}(\theta, T) - Q_{\text{iso}}(0, T)], \quad (9)$$

up to coverage unity, and for several values of reduced temperature T/V_2 for two interaction sets: $V_2 = 1700$ K, $R = 0.1$, $R' = 0.05$ (fig. 6a) and $V_2 = 1200$ K, $R = 0.2$ (fig. 6b). We note that the rises and sudden drops of $\Delta \hat{Q}_{\text{iso}}$ with increasing θ , at low temperature, signal the existence of ordered phases [25]: in fig. 6a the $(\sqrt{3} \times \sqrt{3})R30^\circ$

ordering (drops at $\theta = 1/3$ and $\theta = 2/3$) induced by nearest neighbor repulsion occurs, in addition to the orderings of $p(2 \times 2)$ ($\theta = 1/4$ and $3/4$) and $p(2 \times 1)$ ($\theta = 1/2$) induced by the next-nearest neighbor interaction [26]. We note that these results are consistent with the known $(\sqrt{3} \times \sqrt{3})R30^\circ$ and possible CO/Rh(111) (2×2) structures at $\theta = 1/3$ and $\theta = 1/4$, respectively. In fig. 6b, where the next-nearest neighbor interaction is relatively stronger, the (2×2) and (2×1) phases have completely supplanted the $(\sqrt{3} \times \sqrt{3})R30^\circ$ phase. However, the high temperature behavior of the heat of adsorption, and hence $E_d(\theta, T)$, is essentially the same for both interaction sets, reflecting the similarity of the fits to the experimental isosteres at desorption temperatures. From a more detailed version of fig. 6a we estimate the disappearance of the $(\sqrt{3} \times \sqrt{3})R30^\circ$ structure at $\theta = 1/3$ occurs for $T/V_2 = 0.175 - 0.200$. For $V_2 = 1700$ K this gives an order-disorder temperature at $T = 300 - 340$ K, again entirely consistent with the observed value of 325 K deduced from fig. 1.

4. Monte Carlo calculations: discussion

Here we provide a brief description of the Monte Carlo calculations and results. In the Monte Carlo simulation we considered a triangular lattice gas model [27–30] of $N = 3600$ sites with periodic boundary conditions. The Hamiltonian was the same as eq. (5), with nearest neighbor and next nearest neighbor interactions only taken into account (i.e., $V''_2 = 0$). The root mean square order parameter m_{RMS} (defined in ref. [30]) versus $k_B T / |V_2|$ was calculated at $\theta = 1/3$ for each R value considered in the desorption rate calculations, and the absolute magnitudes of V_2 and V'_2 were adjusted to match the predicted decrease in m_{RMS} at 325 K corresponding to loss of ordering. We obtained equilibrium configurations for fixed values of θ and T (canonical ensemble) from which we calculated the total interaction energy E_i by applying a hopping algorithm and convergence criteria which have been previously described [31–36]. The final desorption rates, k , were then calculated following the

standard procedure: the transition probability for desorption is such that one counts the number of occupied sites neighbouring the desorbing particle, and weights the desorption rate for this particle by the Boltzmann factor generated by the interaction energy due to these neighbors, i.e.,

$$k = [v_0 \exp(-E_0/k_B T)] \exp(E_i/k_B T) \quad (10)$$

where the factor in square brackets is the Arrhenius form for the desorbing particle.

We have found that the best Monte Carlo results (i.e., closest to experimental results) do not demonstrate the same accuracy that has been achieved by the use of eq. (1), combined with the transfer matrix method. Nevertheless, both nearest neighbor and weaker next-nearest neighbor repulsions were required for the Monte Carlo fits to structural data, and of relative strength similar to that deduced above. However a caution regarding the application of this technique is in order: by the principle of detailed balance, the desorption rate (10) implies an adsorption transition rate with a sticking coefficient $S(\theta) = 1 - \langle n_i \rangle \rightarrow 1 - \theta$. Thus in any system where the sticking coefficient does not follow this simple law, simulation of desorption rates by the standard Monte Carlo procedure (i.e., employing eq. (10)) is inappropriate. Thus the inability to fit the data for the CO/Rh(111) system is not surprising. Clearly for other systems for which the $S(\theta) = 1 - \theta$ assumption is valid, the two methods generate identical results.

5. Conclusion

Our theoretical analysis of desorption of CO from Rh(111), combining a transfer matrix calculation of the adsorbate chemical potential with a model of desorption under quasi-equilibrium conditions, has met with considerable success. These calculations have been compared with linearized and essentially isosteric desorption rates that were obtained using a three molecular beam arrangement. We have been able to fit accurately all the experimentally determined desorption isosteres and, in so doing, deduce a set of interaction parameters for the CO molecules, comprising a

strong (relative to $k_B T$) nearest neighbor and weaker next-nearest neighbor repulsion, and an attractive third-nearest neighbor attraction: $V_2 = 3.38$ kcal/mol, $V_2' = 0.1 V_2$, $V_2'' = -0.05 V_2$, with an uncertainty of order 10%. In addition, these parameters predict structural features for CO/Rh(111) at temperatures well below the desorption range which are consistent with the diffraction data. In particular, we find a range of temperatures for the ordering into the $(\sqrt{3} \times \sqrt{3})R30^\circ$ structure at coverage $1/3$ which contains the transition temperature observed in the He diffraction measurements. Also, the low temperature (2×2) structure at coverage $1/4$, observed in the LEED experiments [24], is predicted. Previous estimates of possible interaction parameter sets by Kjoll et al. for this system are inconsistent with the experimental desorption data.

Sets of nearest and next-nearest interactions were also deduced by Monte Carlo simulations of the observed ordering temperature for the $(\sqrt{3} \times \sqrt{3})R30^\circ$ structure. However, a standard Monte Carlo calculation of the desorption rate using these values failed to describe the desorption data as accurately as the model above, principally because this standard method is only applicable to systems for which the sticking coefficient has the simple form $(1 - \theta)$.

There are a number of ways that the model parameters can be refined or confirmed. Diffraction measurements carried out at $\theta < 1/3$ and $T < 325$ K can be used to map out the rest of the phase diagram, which can be compared with that already calculated by Roelofs et al. (see fig. 10.8 of ref. [10]) for the interaction ratios $R = 0.1$ and $R' = 0.05$. In addition, measurements of the isosteric heat of adsorption, which is independent of sticking, as well as further measurements of TPD and isothermal desorption rates, should be made to help confirm these ratios. Our attempts to match TPD spectra above $\theta = 1/3$ (which appear in ref. [24]) fail with our present model, as we have not allowed for occupation of an additional binding site. On Rh(111), CO competes for both on-top and bridge sites [14,15,37], with binding at lower coverages occurring at on-top sites and at higher coverages at both on-top and bridge sites. Calculations to account for this

effect and model higher coverage ($\theta > 0.22$) desorption are in progress. A study of the general features expected for desorption of particles from a triangular lattice with predominantly repulsive nearest neighbor interactions, as calculated using the method of section 3, will be presented elsewhere [38].

Acknowledgements

S.H.P. and H.J.K. acknowledge support from the Network of Centres of Excellence Programme in association with the Natural Sciences and Engineering Research Council of Canada. K.A.P., T.J.C., and S.J.S. acknowledge support from the Office of Naval Research and by the NSF Materials Research Laboratory at The University of Chicago.

References

- [1] H. Pfnür and D. Menzel, *J. Chem. Phys.* 79(5) (1983) 2400.
- [2] H. Pfnür and D. Menzel, *J. Chem. Phys.* 79(9) (1983) 4613.
- [3] B.J. Hinch and L.H. Dubois, *Chem. Phys. Lett.* 171 (1990) 131.
- [4] C.T. Rettner, D.S. Bethune and E.K. Schweizer, *J. Chem. Phys.* 92 (1990) 1442.
- [5] L.D. Peterson and S.D. Kevan, *Surf. Sci. Lett.* 235 (1990) L285.
- [6] For a review, see: E.G. Seebauer, A.C.F. Kong and L.D. Schmidt, *Surf. Sci.* 193 (1988) 417.
- [7] K.J. Wu and S.D. Kevan, *J. Chem. Phys.* 95 (1991) 5355.
- [8] U. Leihäuser, *Z. Phys. B.* 37 (1980) 65.
- [9] D.M. Burley, in: *Phase Transitions and Critical Phenomena*, Vol. 2, Eds. C. Domb and M.S. Green (Academic Press, New York, 1972) p. 329.
- [10] L.D. Roelofs, in: *Chemistry and Physics of Solid Surfaces IV*, Eds. R. Vaneslow and R. Howe (Springer, Berlin, 1982) p. 219.
- [11] L.D. Roelofs and R.J. Bellon, *Surf. Sci.* 223 (1989) 585.
- [12] P.A. Rikvold, J.B. Collins, G.D. Hansen and J.D. Gunton, *Surf. Sci.* 203 (1988) 500.
- [13] N.C. Bartelt, T.L. Einstein and L.D. Roelofs, *Phys. Rev. B* 34 (1986) 1616.
- [14] K.A. Peterlinz, T.J. Curtiss and S.J. Sibener, *J. Chem. Phys.* 95 (1991) 6972.
- [15] L.H. Dubois and G.A. Somorjai, *Surf. Sci.* 91 (1980) 514.
- [16] D.F. Padowitz and S.J. Sibener, *J. Vac. Sci. Technol. A* 9 (1991) 2289.
- [17] D.F. Padowitz and S.J. Sibener, *Surf. Sci.* 254 (1991) 125.
- [18] D.F. Padowitz, K.A. Peterlinz and S.J. Sibener, *Langmuir* 7 (1991) 2566.
- [19] H.J. Kreuzer and S.H. Payne, in: *Dynamics of Gas-Surface Interactions*, Eds. C.T. Rettner and M.N.R. Ashfold (R. Soc. Chem., Cambridge, 1991) p. 220.
- [20] N.H. Fuchs, *Phys. Rev. B* 41 (1990) 2173.
- [21] P.A. Rikvold, K. Kaski, J.D. Gunton and M.C. Yalabik, *Phys. Rev. B* 29 (1984) 6285.
- [22] W. Kinzel and M. Schick, *Phys. Rev. B* 23 (1981) 3435.
- [23] J. Kjoll, T. Ala-Nilisa and S.C. Ying, *Surf. Sci.* 214 (1989) 448.
- [24] P.A. Thiel, E.D. Williams, J.T. Yates, Jr. and W.H. Weinberg, *Surf. Sci.* 84 (1979) 54.
- [25] S.H. Payne, H.J. Kreuzer and L.D. Roelofs, *Surf. Sci. Lett.* 259 (1991) L781.
- [26] J.S. Walker and M. Schick, *Phys. Rev. B* 20 (1979) 2088.
- [27] K. Wada, T. Tsukuda and T. Ishikawa, *J. Phys. Soc. Jpn.* 52 (1983) 1531.
- [28] S. Fujihi, S. Shuth, Y. Abe and S. Katsura, *J. Phys. Soc. Jpn.* 52 (1983) 1531.
- [29] B. Mikura and D.P. Landau, *Phys. Rev. Lett.* 38 (1977) 977.
- [30] D.P. Landau, *Phys. Rev. B* 27 (1983) 5604.
- [31] M. Tringides and R. Gomer, *Surf. Sci.* 145 (1984) 121.
- [32] M. Tringides and R. Gomer, *Surf. Sci.* 166 (1986) 419.
- [33] C. Uebing and R. Gomer, *J. Appl. Phys.* 69 (1991) 8.
- [34] C. Uebing and R. Gomer, *J. Chem. Phys.* 95 (1991) 7626.
- [35] A.B. Bortz, M.H. Kalos, J.L. Lebowitz and M.A. Zendejas, *Phys. Rev. B* 10 (1974) 535.
- [36] K. Binder and D.P. Landau, *Surf. Sci.* 61 (1976) 577.
- [37] M.A. Van Hove, R.J. Koestner, J.C. Frost and G.A. Somorjai, *Surf. Sci.* 129 (1983) 482.
- [38] S.H. Payne, Zhang Jun and H.J. Kreuzer, *Surf. Sci.* 264 (1992) 185.